Soft Matter

ARTICLE

# Ordering of colloidal hard spheres under gravity: From monolayer to multilayer

Received 00th January 20xx,
Accepted 00th January 20xx

DOI: 10.1039/x0xx00000x

www.rsc.org/

Ziwei Guo [a], Peiyao Wu [a] and James T. Kindt * [a]

The phase behaviour of hard spheres confined by a gravitational potential to a thin layer (up to several monolayers) near a hard, flat surface is investigated using grand canonical Monte Carlo simulation. Depending on the strength of the gravitational field, the bottom monolayer of spheres may adopt uniform hexagonal order before, during, or after the growth of the second layer of particles. The crossover from ordering with a sparsely populated overlayer to ordering with almost one-third of the system's particles forming a second layer is observed upon decreasing the dimensionless Péclet number Pe = $mg\sigma/k_BT$ from 18 to 16. The particular sensitivity of the nature of the transition to particle size in this range is interpreted in terms of competing influences on the base layer structure by particles in the overlayer: promotion of order through increased pressure, versus stabilization of defects through occupation of low-lying sites on top of them. Simulations of grain boundaries between 2-d ordered domains of different orientation are used to correlate the degree of overlayer coverage to its effects on grain boundary stiffness as an indicator of defect free energy. Finally, we examine the structure of the ordered phases at coexistence over a range of gravitational strengths and find that orientational ordering of the second monolayer occurs along with first-order transition of the base layer at Pe=8 but not at Pe=10.

## 1. Introduction

When packed at high enough lateral densities, hard spheres confined to a plane undergo a transition to a hexagonally ordered state, in a process that has been studied for decades through theory and computation.[1] Only recently have computer simulations on large systems been able to describe this transition unambiguously as a two-stage process: a discontinuous transition from a fluid to a hexatic liquid crystalline structure followed by a continuous transition to a 2-d solid.[2] Even more recently, this two-stage process has been observed in experiments on monolayers of confined spherical colloidal particles.[3] Ordered arrays of colloidal particles in two and three dimensions may be prepared via a variety of routes[4] and find applications in optics, electronics, and sensing.[4] Surface tension effects frequently drive colloids to adsorb strongly to interfaces between immiscible fluids, forming Pickering emulsions.[5-7] Although colloidal monolayers at hard surfaces or fluid interfaces may interact via a wide range of direct and interfacially-mediated (e.g. capillary) forces, at high enough lateral densities simple steric effects are likely to dominate these interactions and hard-sphere (HS) models become relevant.

This work builds on the now well-understood behaviour of the ordering transition of HS in a purely 2-d environment to address questions about this ordering under a gravitational field for sedimented particles. The ordering of sedimented HS in the multilayer limit under mild gravitational confinement has been studied in depth,[8-16] as has the quasi-2d phase behaviour of HS under confinement between hard walls.[17-20] In systems of sedimenting particles, the Péclet number ($\mathrm{Pe} = mg\sigma/k_BT$, equivalent to $g^*$ or $1/l_g$) is equivalent to the gravitational potential energy in units of $k_BT$ required to raise the particle by a distance of its diameter $\sigma$. Using the buoyant density of silica spheres in water at 300 K as an example, the conversion from Pe to diameter is Pe = 2.06 $\mu\mathrm{m}^{-4}\sigma^4$. (It has been noted[9] that an alternate definition of the Péclet number at $\mathrm{Pe} = (\Delta\rho)gR^4/k_BT$ also appears in the literature[15, 16] and gives a value 8 times less.) A recent computational and experimental study[21] has been made of structure and dynamics of colloidal monolayers under a moderate Pe (=6.3), but like earlier simulation work on the subject[22] it stopped short of any ordering transitions. Marechal and Dijkstra have used grand canonical Monte Carlo simulation to study ordering in HS multilayers under gravity, showing among other things that simultaneous freezing of the lowest two layers is a first-order transition in the range Pe=1-4, but that at Pe=10 the ordering of the second layer proceeds continuously after the freezing of the base layer,[13] a result that was corroborated through experiment.[23]

As spheres are added to the system they may either (roughly speaking) increase the density of the lowest level at a cost in packing entropy or occupy positions on top of this lowest level at a cost in gravitational energy. At high Pe, we do not expect significant population above the base layer until the base layer is densely packed and in the 2-d solid state. Thorneywork *et al.* demonstrated this behaviour in showing that monolayers of colloidal spheres with Pe=41 undergo two-stage melting at densities close to the transitions derived from simulations of of hard disc (HD) systems.[3] For more weakly confined particles, the lateral pressure in the base layer may

[a] Department of Chemistry, Emory University, Atlanta, GA, 30322, USA.
E-mail: jkindt@emory.edu
Electronic Supplementary Information (ESI) available. See DOI: 10.1039/x0xx00000x

be high enough to push particles to the second level before the hard disk (HD) ordering transition is reached. Using results from our previous work,[24] we can estimate the critical value of Pe at which the crossover takes place. The cost in gravitational energy to add to a second layer above a close-packed monolayer is $\sqrt{2/3}$ (=0.816) Pe $k_BT$. The entropic cost to add a particle to a densely packed, ordered monolayer can be estimated from 2-d HD simulations[24] where the ordering transition occurred at a chemical potential of 12.8 $k_BT$/molecule. These are equal when Pe=15.6; we may estimate that above this value (which corresponds to 1.66 μm diameter spherical silica beads in water at 300 K), ordering of the base layer will precede population of the overlayer. For particles with Pe below this threshold, as increasing numbers of particles accumulate in one or more upper layers, their weight will eventually produce enough pressure to drive an ordering transition in the base layer (or layers). A main goal of this work is to test this prediction through simulation.

The phase behaviour of HS confined to a slit pore with hard walls has been studied extensively through simulation[18-20, 25] and experiment[17, 26, 27] and bears some similarity to the gravitationally confined systems to be modelled here. Particles held in soft confinement near a plane through a harmonic potential[28] have also been studied. At high packing density, these systems may adopt ordered structures with integer numbers of planar hexagonal (triangular) or square arrays; more complex intermediates (e.g. buckled structures) are also observed under hard wall confinement, while re-entrant melting or phase coexistence is seen under soft confinement. The non-hexagonal packing modes are driven by a trade-off between packing efficiently within a plane while accommodating multiple layers. In the present system, the broken symmetry between layers makes optimization of the packing efficiency in the base layer the most important factor, so we expect to see only hexagonally symmetric ordered structures.

In this work, we explore gravitationally confined HS monolayers and bilayers with a relatively high range of Pe from 6 to 24. Here we use the solvent repacking Monte Carlo (SRMC) method,[24] along with a new extension adapting the simulation under a gravitational potential, to study the equilibrium phase diagrams and properties of gravitationally confined HS. The effects of overlayer on the thermodynamics of disordering are then singled out using studies of grain boundary (GB) stiffness. Finally, we address the structural nature of ordering in the ordered phase at coexistence in different limits.

## 2. Methods

### 2.1 Algorithms for grand canonical Monte Carlo under a gravitational potential

We treat a monodisperse system of HS whose minimum centre-of-mass position along $z$ is limited to $z = 0$ by a hard, flat surface in the *x*-*y* plane ("floor") and whose maximum position along $z$ is influenced by a gravitational potential $U = \mathrm{Pe}\, k_BTz$ and limited to $z_{max}$ by a second hard wall ("ceiling"). We wish to establish an equilibrium between this system and a reference system of fugacity $f$, which can be characterized as a hypothetical non-interacting system of particles in a field-free 3-d space ($U = 0$) at a number density $f$ in units of $\sigma^{-3}$.

### 2.2 Single particle addition/removal moves

The standard Grand Canonical Monte Carlo algorithm for such a system would be inefficient at high Pe and high $z_{max}$ because most insertion move attempts would be at heights with low thermal population. Biasing the distribution of insertion attempts by the gravitational potential is a natural solution. Given the normalized probability distribution $P(z) = \mathrm{Pe}\, e^{-\mathrm{Pe}\, z}/(1 - e^{-\mathrm{Pe}\, z_{max}})$, acceptance probabilities that would appropriately account for the bias can be easily constructed:

$$acc_{N\to N+1} = \min\left(1, \frac{f\frac{V}{N+1}e^{-\mathrm{Pe}\, z}}{P(z)}\right) = \min\left(1, f\frac{V}{N+1}\frac{(1-e^{-\mathrm{Pe}\, z_{max}})}{\mathrm{Pe}}\right) \quad (1a)$$

$$acc_{N+1\to N} = \min\left(1, f^{-1}\frac{N+1}{V}\frac{\mathrm{Pe}}{(1-e^{-\mathrm{Pe}\, z_{max}})}\right) \quad (1b)$$

For a system that is densely packed near $z = 0$ at high Pe, this will again produce inefficiencies because the insertion moves will be concentrated at the most densely packed region. To increase the rate of exchange for the uppermost layer at least, while retaining the possibility of inserting into cavities that open up near $z = 0$, we instead bias insertions according to the gravitational potential but over a range determined by a "local floor" using the following steps:

1) A point within the *x*-*y* plane is selected at random.
2) The positions of all particles whose *x*, *y* coordinates are in a cylinder of radius $\sigma$ centered at that point are used to calculate the height $z$ at which a particle falling from $z_{max}$ would first collide with the existing particles; this is denoted $z_{floor}$. If there are no particles within that cylinder, $z_{floor} = 0$. If a particle at $z_{max}$ would overlap with an existing particle, the move fails.
3) The trial $z$ coordinate is selected from the range $[z_{floor}, z_{max}]$, with probability weighted by $e^{-\mathrm{Pe}\, z}$.

The acceptance probability for insertion moves is then

$$acc_{N\to N+1} = \min\left(1, f\frac{V}{N+1}\frac{\left(e^{-\mathrm{Pe}\, z_{floor}} - e^{-\mathrm{Pe}\, z_{max}}\right)}{\mathrm{Pe}}\right) \quad (2)$$

We note that this move can never insert a particle underneath another particle.

For the removal move,

1) One of $N + 1$ particles is selected at random. The positions of all particles whose *x*, *y* coordinates are in a cylinder of radius $\sigma$ centered at that particle's projection on the *x*, *y* plane are used to calculate both $z_{floor}$ and $z_{ceiling}$: the positions at which the particle would make contact (with walls or other particles) if it were to fall or rise without changing lateral position.
2) If $z_{ceiling}$ is less than $z_{max}$, there is another particle above our trial particle, and the move fails because it could not be reversed by an on-top addition and so would violate detailed balance.
3) The acceptance probability for removing the selected particle is

$$acc_{N+1\to N} = \min\left(1, f^{-1}\frac{N+1}{V}\frac{\mathrm{Pe}}{\left(e^{-\mathrm{Pe}\, z_{floor}} - e^{-\mathrm{Pe}\, z_{max}}\right)}\right) \quad (3)$$

If the removal move fails for either reason (either because the particle has another one above it, or because the acceptance probability is less than 1), knowing $z_{floor}$ and $z_{ceiling}$ allows us to make a rejection-free move along $z$, translating the particle to a

 

position between these two values with a probability weighted by $e^{-\mathrm{Pe}\,z}$. This move is appealing in that the effective step size adapts automatically both to the local packing environment and the gravitational confinement, removing the need to re-optimize the step size to sample height distributions efficiently. The thermal distribution for an ideal (non-interacting) system under the gravitational potential with fugacity defined in this way would be:

$$\rho_{3d}(x,y,z) = f\exp(-\beta U) = f\exp(-\mathrm{Pe}\,z) \quad (4)$$

Integrating $\rho_{3d}(x,y,z)$ over $z$ then yields a number per unit area of $f(1-e^{-\mathrm{Pe}\,z_{max}})/\mathrm{Pe}$. The single-particle on-top insertion and removal moves are in principle valid at any value of Pe, although for multilayer systems their ability to converge to the correct ensemble of particle numbers and configurations at a given fugacity relies on the efficient exchange of particles within and between layers below the top layer, through local moves.

### 2.3 Solvent Repacking MC Moves under gravitational potential

The SRMC algorithm has been detailed in several publications.[24, 29] In the present system, the goal of the algorithm is to allow a local region of the system to adopt a new packing that might be kinetically inaccessible through single-particle moves. Disorder in the base layer can be stabilized by the presence of overlayer particles, and so in principle trial configurations that allow both layers to be altered simultaneously could overcome barriers to structural transitions.

Like in previous work on 2-d systems, a position is randomly selected within the system and a set of trial configurations is generated in which all particles within a lateral distance $r_{\mathrm{cut}}$ are replaced with varying numbers of particles, whose positions are chosen using the configurational bias MC (CBMC) strategy.[30] In the present case, we wish to build a configuration of particles that may extend to a second layer (or beyond) with guidance from the gravitational potential energy. As before, for the *i*'th particle added to the new trial configuration, a number *k* of positions in *x* and *y* are generated randomly within the circle of area $\pi r_{\mathrm{cut}}^2$. For each position, the local floor $z_{floor}$ is calculated as defined above, except that only interactions with the previous *i*-1 particles in the new configuration (not with the surrounding "shell" particles that may overlap with trial positions) are used for this calculation. The new particle's $z$ coordinate is selected with an exponentially biased distribution ($\propto e^{-Pe\,z}$) between $z_{\mathrm{floor}}$ and $z_{\mathrm{max}}$. Trial positions that overlap shell particles are rejected, and one of the remaining positions is selected with a probability weighting

$$P_{i,j} = \frac{e^{-\beta u'_{i,j}}\left(e^{-Pe\,z_{floor,i,j}} - e^{-Pe\,z_{max}}\right)}{\sum_{j'=1}^{k} e^{-\beta u'_{i,j'}}\left(e^{-Pe\,z_{floor,i,j'}} - e^{-Pe\,z_{max}}\right)} = \frac{e^{-\beta u'_{i,j}}\left(e^{-Pe\,z_{floor,i,j}} - e^{-Pe\,z_{max}}\right)}{w_i} \quad (5)$$

where $u'_{i,j}$ is an auxiliary potential, derived from a radial distribution function, that favours closely packed positions, and a Rosenbluth weight $w_i$ associated with the placement of the *i*th particle is introduced. (The same auxiliary potential was used here as in previous work.[29, 31]) Particle addition is continued until either a predetermined maximum is reached or all positions generated are invalid ($z_{\mathrm{floor}} > z_{\mathrm{max}}$).

A complication arises as we need to account for the probability of generating a given set of *i* particle positions in this manner, including permutations to the order in which they may be generated. If no particle is above any other particle (in the sense that $z_{\mathrm{floor}} = 0$ for all), then the number of permutations equals *i* factorial. In the event that some particles are on top of others, some of these permutations violate the ordering requirement for particles to be inserted earlier than those that are on top of them. To sample and count the allowed permutations for a given arrangement of *i* particles, we first count the number $n_{\mathrm{top},i}$ of particles that have no particles below them, randomly select one to remove, and continue recounting until a single particle is left. The product of $n_{\mathrm{top},i}$ :

$$N_{perm,i} = \prod_{i'=1}^{i} n_{top,i'} \quad (6)$$

will equal the number of permutations, and so is used in place of *i*! in expressions for the acceptance probability. The probability weighting associated with the configuration $\mathrm{r}^i$ of *i* particles within the grand canonical ensemble is

$$P(\mathrm{r}^i) \propto \frac{f^i}{\Lambda^i}\exp\left(-Pe\,\sum_{i'=0}^{i} z_{i'}\right) \quad (7)$$

The probability of generating that given configuration (including selecting lateral positions for *i* particles from an area $a_{\mathrm{cav}} = \pi r_{\mathrm{cut}}^2$, generating *z* coordinates from the gravitationally biased distribution between $z_{\mathrm{floor}}$ and $z_{\mathrm{max}}$, and selecting one of *k* positions according to eqn. 7) is:

$$\alpha(\mathrm{r}^i) = N_{perm,i}\prod_{i'=1}^{i}\left(\frac{k_{i'}}{a_{cav}}\right)\left(\frac{Pe\;e^{-Pe\,z_{i'}}}{e^{-Pe\,z_{floor,i'}} - e^{-Pe\,z_{max}}}\right)\frac{e^{-\beta u'_{i'} - Pe\,z_{floor,i'}}}{w_{i'}} \quad (8)$$

Acceptance probability weightings for moves in biased Monte Carlo algorithms should be proportional to the desired weighting within the ensemble and inversely proportional to the generation probability; dividing eqn. 8 by eqn. 5 yields the acceptance probability weighting of the new configuration with *i* particles:

$$\omega_i = \frac{f^i}{\Lambda^i}\frac{{a_{cav}}^i}{N_{perm,i}\prod_{i'=1}^{i} k_{i'}}\frac{\prod_{i'=1}^{i} w_{i'}}{\exp\left(-\beta U_i'\right)} \quad (9)$$

As in conventional CBMC, all factors in eqn. 9 for the original (old) configuration must also be generated, using *k*-1 "dummy" alternate positions for each particle positioned to generate $w_{i,\mathrm{old}}$ according to eq. 7 and adding new additional "dummy" particles up to the same stopping criterion as for the new structure. The acceptance probability for choosing one of the new structures is then:

$$acc = \min\left(\frac{\sum_{i=0}^{i^{max}}\omega_i}{\sum_{i'=0}^{i^{max}}\omega_{old,i'}}, 1\right) \quad (10)$$

If the move is accepted, the choice of how many of the particles to include in the new filling of the cavity (including the vacant cavity, *i*=0, with weight 1) is made through a random selection with probability:

$$P(i) = \frac{\omega_i}{\sum_{i'=0}^{i^{max}}\omega_{i'}} \quad (11)$$

### 2.4 Implementation of grand canonical Monte Carlo (GCMC) simulations

GCMC simulations with varying fugacities *f* and Péclet numbers Pe were carried out through the moves described above using a grid-based domain decomposition scheme in which the system (a square box with periodic boundary conditions in two dimensions, whose size depended on the type of simulation as detailed below) is divided into $n \times n$ sectors. During each cycle, a new origin for the first sector of the grid is selected at random and a series of Monte Carlo moves attempts is performed independently on a different processor on each sector, with boundary zones of width $1\sigma$ between the sectors kept unchanged (with no particles allowed to enter, leave, or change position). A single cycle consisted of 1000 SRMC repack attempts on each sector, each of which was followed by 600 single-particle move attempts. The type of single-particle move was randomly selected with equal chances of a simple lateral translational move attempt at constant *z*, a single-particle (on-top) insertion attempt, or a single particle removal / rejection-free vertical translation move as described above.

To determine the boundaries between ordered and disordered phases in systems with Pe numbers ranging from 6 to 24, a simulation box of lateral dimensions $100\,\sigma \times 100\,\sigma$ was used, divided laterally into 16 sectors for parallel sampling. At each value of Pe, we use an estimation and trial strategy to find the transition point. Starting from an empty box, simulations were performed at widely spaced trial fugacities, and the total particle number was monitored until it reached a stable level. This typically was achieved within 5,000-10,000 MC cycles (with each MC cycle including a total over all sectors of 16,000 repacking moves attempts and $9.6 \times 10^6$ single-particle move or insertion/removal attempts). The base layer (defined as particles with $z < 0.5\,\sigma$, where $z = 0$ represents the particle in contact with the hard surface) was visualized using VMD[32] to determine whether it had reached a state of uniform hexagonal order. The structure at the lowest fugacity to yield an ordered state was then used as input for a series of simulations at gradually decreasing fugacity, until a system was observed in which the uniform order of the base layer was lost (melted). Simulations initiated with disordered structures were then performed at smaller increases of fugacity (increments of 5-10%) until ordering was resumed. In this way we zeroed in on a transition fugacity value – where the same fugacity will result in the ordered structures remaining ordered and the disordered structures remaining disordered over a 10,000 MC cycle trajectory. Although there is some imprecision in this procedure, as the range of the bistable regions is finite for a finite equilibration time, the outer limits of this range (which we could place by the fugacities at which spontaneous transitions were observed) were far narrower than the shifts in the transitions from varying Pe. The properties of the two phases at coexistence are then approximated from the configurations observed at that transition fugacity obtained using different starting structures. To represent the density of the system with a measure that reduces to the 2-dimensional area fraction in the limit of a monolayer at infinite Pe, the total area fraction $\eta_{tot} = \frac{\pi}{4}\frac{<N>}{A}$ is used, representing the mean sum of all projected areas of all spheres in the system as fraction of the area of the surface. (This measure can exceed 1 because of the possibility of multiple layers). The area fractions $\eta_{base}$ and $\eta_{over}$ of the base layer (particles with $z < 0.5\sigma$) and the first overlayer (particles with $0.5\sigma < z < 1.5\sigma$) are similarly defined. A list of the transition fugacities and corresponding area fractions of ordered and disordered systems obtained in given in Table S1 in the Supplementary Information section.

With one exception, the ceiling height was set to $z_{max} = 5\sigma$; the choice of this maximum is large enough that the density of particles at or above this height is close to zero and should have negligible effects on the results presented. In one case, at Pe=8, an additional series of simulations was performed using ceiling height $z_{max}$ = $0.5\sigma$ to confine the particles in the system to the first layer, and the transition fugacity of such a system (where overlayer formation is effectively curtailed) was determined in the same manner as above.

To systematically study the GB stiffness and its dependence on system composition and Pe under controllable conditions, ordered grains of spheres are set up in a pair of parallel stripes making two parallel GBs aligned with the $x$ direction in a square simulation box (side length 200 $\sigma$) as in previous work.[29, 31] Equilibration and production periods consisted of at least 5000 and 20000 MC cycles, respectively.

### 2.5 Analysis of orientational and translational order

At each value of Pe, the complex hexagonal bond orientation order parameter $\Psi_6$ was determined for all particles in the base layer ($z < 0.5\sigma$); for systems with Pe=6, 8, and 10 the order parameter was also determined separately for particles in the first overlayer ($0.5\sigma < z < 1.5\sigma$).

$$\Psi_6(\vec{r}_j) = \frac{1}{N_j}\sum_{k=1}^{N_j} e^{i6\theta_{jk}} \qquad (12)$$

Here the number of neighbours $N_j$ is defined as the number of particles within the same layer (base layer or first overlayer) with projected distance from particle *j* in the x-y plane less than 1.5 $\sigma$, and $\theta_{jk}$ is the angle between the *y* axis and the *x-y* projection of the bond vector between particle *j* and its $k^{th}$ neighbour.

Selected systems were prepared in the ordered phase and equilibrated at the transition fugacity in a larger simulation box ($350\sigma \times 350\sigma$) to reduce finite size effects calculation of translational order correlation function following a procedure given in a previous study.[24] The direction of translational correlation vector is chosen based on the orientation of the domain, to obtain the longest possible correlation length.

### 2.6 Grain Boundary detection and calculation of grain boundary stiffness

To detect the two GB's positions along the *x* dimension from simulations of bicrystals, we divide the simulation box into a 100×100 grid, which has been confirmed to be fine enough for calculating interfacial stiffness in our previous study.[29, 31] The orientation of the hexagon formed by six neighbours of particle *j* can be calculated by $\theta_6 = \arg(\Psi_6)/6$, which is a value varied from 0 to 60° due to the symmetry of hexagon, using only particles in the base layer. The orientation of the grain domain can be quantified by averaging all the $\theta_6$ of particles belonging to the domain. Here in all cases GB were constructed with grain misorientation (difference between the two

 

grains' orientation angles) of 30° and inclination (angle between the GB and grain orientations) of 15°. Smoothing over local pockets of disorder is achieved by taking the average of $\theta_6$ in each grid and the four nearest grid squares of the same *x* coordinate to represent the orientation of each grid square. The height *h* of the grain boundary is then the *y* coordinate of the grid square with $\theta_6$ closest to the mean of the $\theta_6$ values of the two grains, defined as the "edge point", and the GB is represented as a sequence of segments connecting "edge points"

The capillary fluctuation method (CFM) is applied here in the same way as in previous work to calculate GB stiffness.[29, 31] The GB positions along the *y* direction determined as described in previous section are treated as a function of position along the $x$ direction and frame $t$: $h(x,t)$. The mean value of $h(x,t)$ at each $t$ is subtracted off to yield the fluctuation at that frame: $\delta h(x,t) = h(x,t) - \langle h(t)\rangle_x$, which can be converted to $\delta h(k,t)$ by Fourier Transform (F.T.) with wave number $k$=$2\pi m/L$ ($m = 0, \pm1, \pm2, \ldots$) in Fourier Spectrum. The trajectory-averaged square of intensities $\langle|\delta h(k)|^2\rangle_t$ are related to the stiffness $\Gamma$ according to the CFM as:[33]

$$\log(\langle|\delta h(k)|^2\rangle L) = -2\log(k) + \log\left(\frac{k_B T}{\Gamma}\right) \qquad (13)$$

In practice, a linear fit of eqn. 13 with a fixed slope –2 is used to find stiffness $\Gamma$ from the *y*-intercept, excluding points with $|m|$ higher than 15, which the CFM as a continuum-based model is not expected to fit. In ordered systems with Pe=10 and below, convergence in GB fluctuation statistics was not reliable and so is not reported.

## 3. Results and discussion

We will first show how the point of transition of the base layer from fluid to ordered phase depends on the degree of gravitational confinement as represented by Péclet number Pe. The second section will focus on interpreting these trends through consideration of the effect of overlayer particles on the ordering of the base layer, which can be studied more directly by examining the property of grain boundary stiffness at packings above the phase boundary. Finally, the evolution of the nature of the ordered phase near coexistence will be considered, including both lateral translational correlations and the degree to which the second and third layers order in concert with the base layer.

### 3.1 Crossover from ordering before stacking to ordering with overlayer present

We first studied the phase transition points of gravitationally confined HS under different Pe. As predicted, we see a shift in behaviour from an ordering transition that precedes population of overlayer sites (at high Pe) to an ordering transition that occurs with significant overlayer population (at low Pe). The transition appears to take place in the range of Pe between 16 and 18, close to our estimate (explained in the *Introduction section*) of 15.6. As shown in Fig. 1, the ordering transition for sedimented HS with relatively high Pe (18 and 24) takes place at a total area fraction $\eta_{tot}$ shifted only slightly from the HD system, since the occupancy of the overlayer is low, (see Fig. 2) and since the vertical fluctuations in the base layer are small. Upon decreasing the Pe from 18 to 16, $\eta_{tot}$ at the transition is dramatically increased, reflecting the presence of a significant (~37%) overlayer. On further lowering of Pe from 16 to 6, $\eta_{tot}$ at the transition gradually increases, reflecting the need for more and more particles in the upper layers to exert sufficient pressure on the base layer to drive the transition.

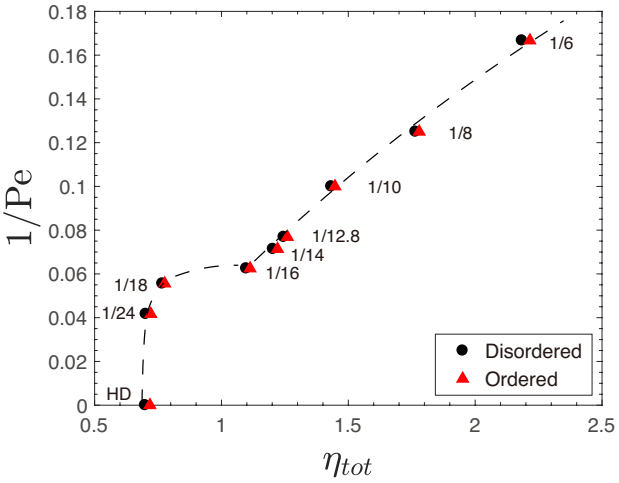


Fig. 1 Phase diagram of gravitationally confined HS systems with different Pe. The dash line is drawn only to guide the eyes to indicate the phase boundaries. The data of HD is obtained from previous work.[24]

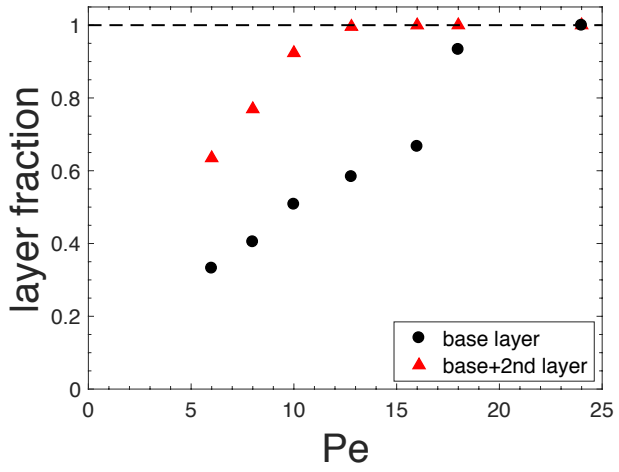


Fig. 2 Percentage of number of base layer particles at phase transition in ordered phase with different Pe.

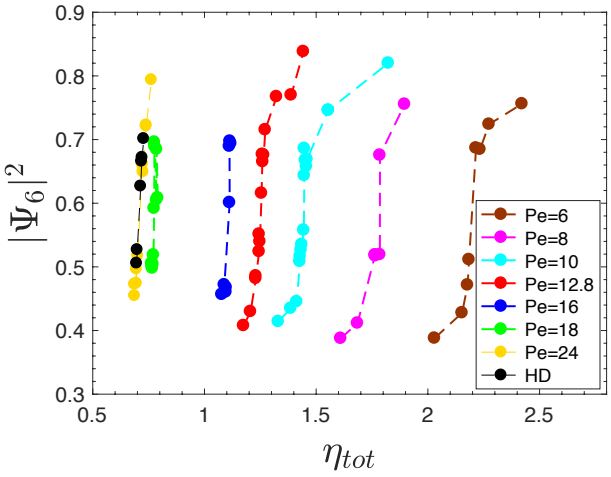


Fig. 3 Mean squared order parameters $\langle|\Psi_6|^2\rangle$ of base layer particles versus total area fraction $\eta_{tot}$ near phase transitions at different Pe.

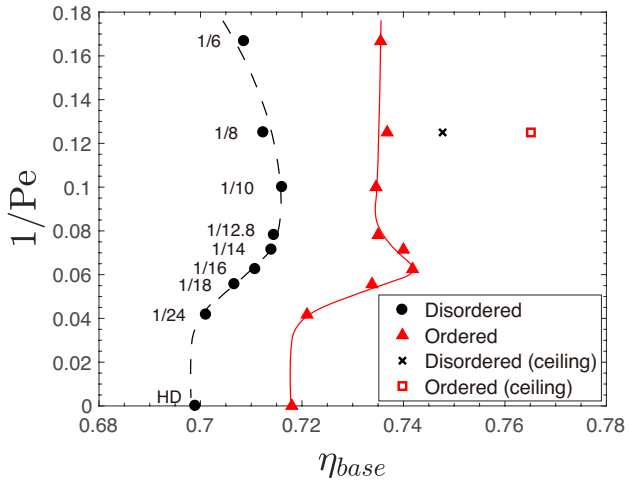


Fig. 4 Phase diagram of gravitationally confined HS systems with different Pe plotted again the base layer area fraction $\eta_{base}$. The lines are drawn only to guide the eyes to indicate the phase boundary in disordered phase (black dash line), and ordered phase (red solid line). The data of HD is obtained from previous work.[24]

### 3.2 Overlayer effects on phase and interface stability

The base layer of HS in the sedimented system differs from the simple HD system in two potentially important ways: the presence of an overlayer and the fluctuations in height (position along $z$) that allow the spheres to approach each other with lateral distances less than their diameter. Over the range of Pe investigated, the boundaries of the ordering transition remain close to the HD limit, in terms of the shift in base layer hexagonal order parameter $\Psi_6$ (Fig. 3) as well as the nominal area fraction $\eta_{base}$ of the base layer (Fig. 4). To distinguish effects of the overlayer from those of the fluctuations, we have simulated the Pe = 8 system under conditions where particles are restricted to a height $z_{max}$ = 0.5$\sigma$ (corresponding to a hard ceiling at a height 1.5 $\sigma$ above the floor). This restriction prevents formation of an overlayer while allowing considerable thermal height fluctuations. The transition boundary is shifted to higher area fraction (cross and square marks in Fig. 4) relative to the HD limit, as expected given the effective softening[34] of the lateral excluded area restrictions due to fluctuations in $z$. This shift is qualitatively consistent with the shifts in phase boundaries observed for HS confined between parallel walls in the absence of a gravitational field.[19] In contrast, when the ceiling is not present, it is noteworthy that the area fraction of the ordered base monolayer at the phase boundary barely changes in the range from Pe=6 to Pe=12.8, remaining near $\eta_{base}$=0.735. (For comparison, the value of $\eta_{base}$ for a monolayer formed by the (111) face of an FCC crystal at the bulk HS freezing point, with volume fraction from simulations[35] determined to equal 0.545, is $\eta$=0.739.) It appears that the doubling in the degree of direct gravitational confinement on the base layer particles and the decrease in the number of particles above the base layer are compensating for each other to produce a consistent packing density in the ordered monolayer at coexistence. This trend is consistent with previous GCMC study that found of similar lattice parameters across ordered phases observed at the transition in the range Pe=1 to 4.[13]

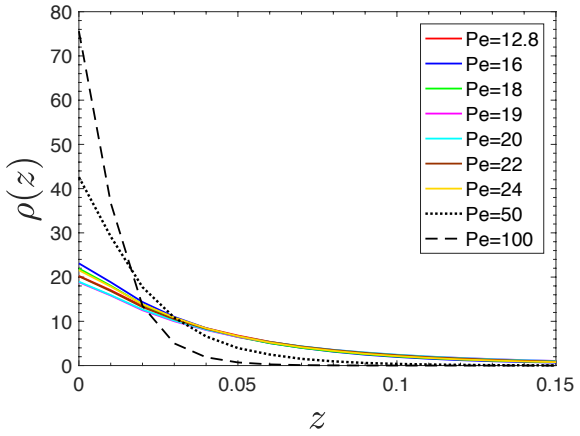


Fig. 5 Height distribution in base layer at common $\eta_{base}$ (~0.755) in base layer with different Pe. $z$ is divided to bins with step size $0.01\sigma$. $\rho(z)$ is the number density per unit volume for spheres in each bin.

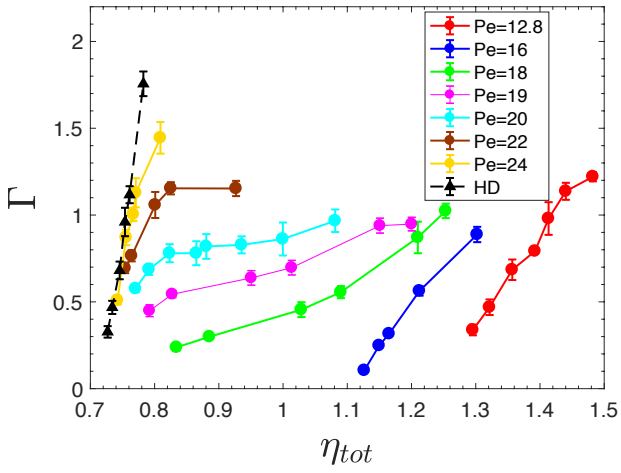


Fig. 6 Stiffness of grain boundaries (assessed using base layer only) with different Pe. The data for HD is obtained from previous work.[29]

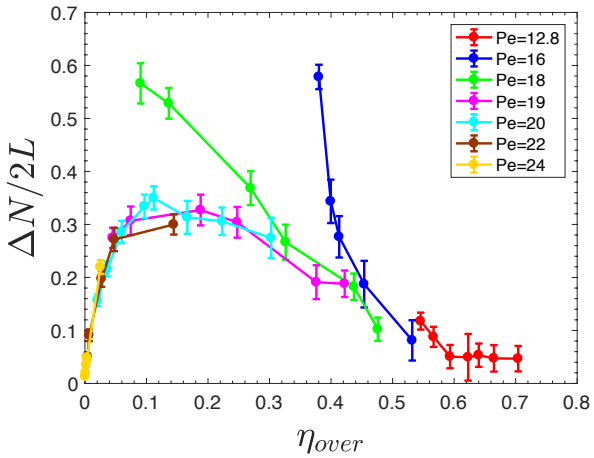


Fig. 7 Excess overlayer particles per unit length of GB at different Pe.

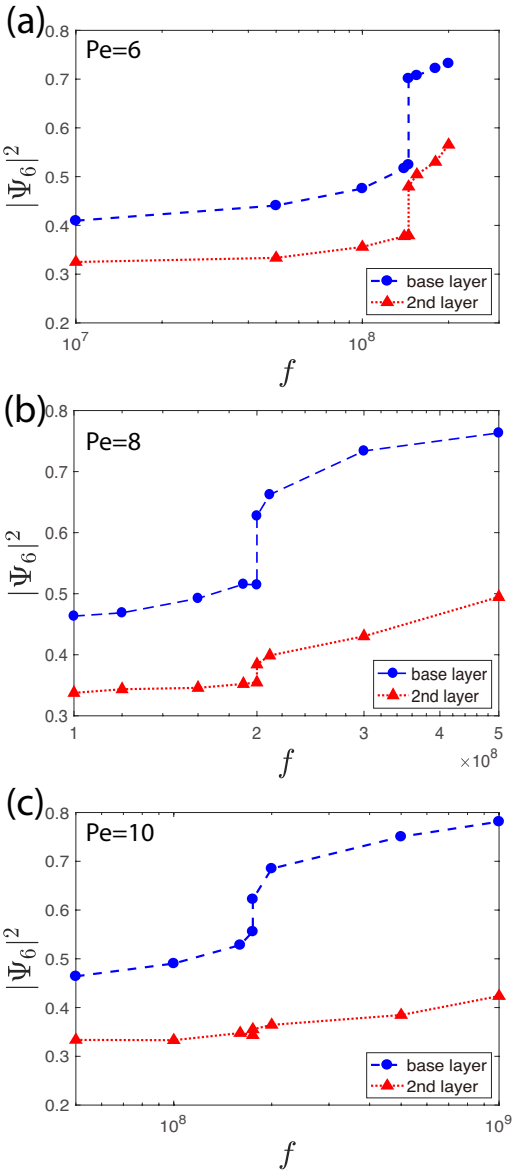


Fig. 8 The hexagonal bond order parameter of spheres in base layer (blue circle) and second layer (red triangle) with (a) Pe=6; (b) Pe=8; and (c) Pe=10.

A related form of compensation is evident in the height distribution of the base layer, shown in Fig. 5, for particles of different Pe under conditions with the same base area fraction ( $\eta_{base}$ ≈0.755, well above the ordering transition). The height distribution broadens as expected when Pe is reduced from 100 to 50 to 24, as gravitational confinement is weakened, then remains approximately unchanged as Pe decreases by another factor of 2. Is this compensation to be expected? In a simplified scenario (neglecting any specific effects of overlayer particles on the base layer packing behaviour) the lateral pressure within the base layer could be assumed to depend solely on $\eta_{base}$. If enough particles are present in the overlayer so that lateral and vertical forces are coupled, this lateral pressure would be expected to be approximately equal to the pressure in the $z$ direction. The pressure on the floor can be equated to $k_BT$ times the number density at $z = 0$ (corresponding to particles whose center is $0.5\sigma$ above the hard surface).[13] Interestingly, even though the height distributions look remarkably similar over the range from Pe=12.8 to Pe=24, the pressure on the floor (as indicated by the density at $z = 0$) shows a spread of about 20%. This indicates that there are subtleties that modulate the dependence of lateral pressure on $\eta_{base}$ and/or that the lateral pressure does not equal the normal pressure. (It would in fact be surprising if the lateral pressure were to equal the normal pressure exactly near a phase coexistence in a thin sedimented system: the lateral pressures of two coexisting phases must be equal to minimize the free energy of the two-phase system, and unless the two phases have the exact same $\eta_{tot}$, they will not have the same normal pressure.) Still, to a first approximation the combination of the direct effect of gravity on the base layer particles and the pressure due to the weight of the overlayers produces a similar height distribution at a given $\eta_{base}$, which in turn would be expected to produce a similar effective 2-d equation of state for the base layer over different values of Pe – absent specific perturbations to the ordering process from overlayer particles. The non-specific effect of increasing overlayer coverage therefore should be expected to favour ordering through its effects on base layer pressure.

To better understand other effects of overlayer coverage on ordering, we turn to the behaviour of grain boundaries, locally disordered regions that separate ordered domains with differently oriented lattices in a polycrystalline system. The fluid phase at the phase transition in HD[2] and similar[36] 2-d systems has some resemblance to a polycrystalline mosaic of locally hexagonal grains with different orientation. In fact, the local hexagonal order is nearly as high as in the fully ordered phase (see Fig. 3) and the correlation length associated with this order is about 60 times the particle diameter for HD systems. Properties of GB might therefore be expected to reflect the factors that control where and how the transition takes place. (GB properties also influence the rate of grain coarsening,[29, 37-39] and are essential for understanding the dynamics of sedimented systems at packings above the ordering transition.) We have compared the (quasi-1d) GB stiffness, which is a measure of the free energy per unit length associated with the GB presence, at different Pe with the HD system (Fig. 6). In the HD limit of a fully 2-d system (Pe=∞), GB stiffness increases sharply with increasing area

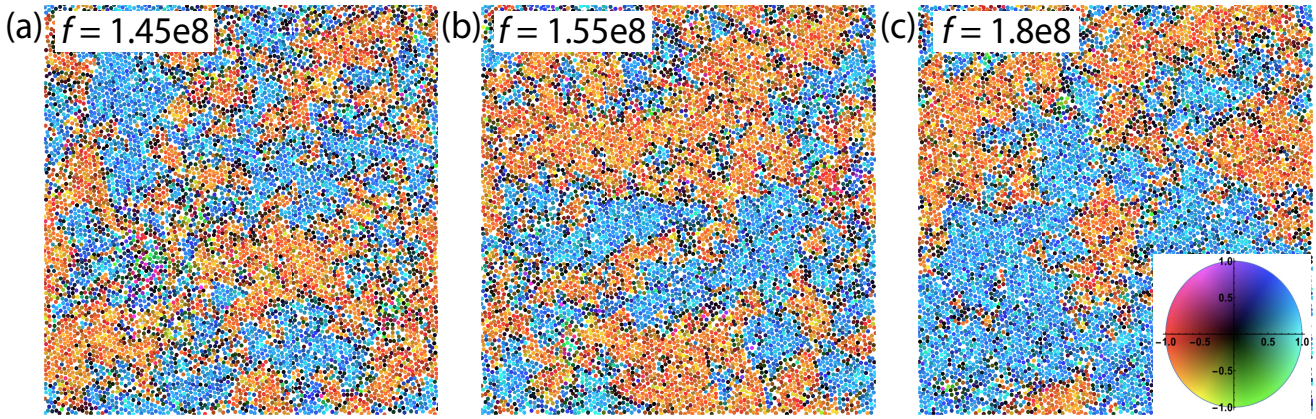


Fig. 9 Snapshot of spheres in the second layer in a system with Pe =6 at fugacity (a) $1.45 \times 10^8$; (b) $1.55 \times 10^8$; and (c) $1.8 \times 10^8$ which are in ordered phase near coexistence. The corresponding total area fractions $\eta_{tot}$ are 2.216, 2.229 and 2.257 respectively. Spheres are colour-coded by order parameter $\Psi_3$ with respect to the spheres in the base layer, represented by the color map shown in the inset in (c); the x and y axes represent the real and imaginary part of $\Psi_3$, respectively.

fraction above the transition.[29] This dependence is weaker over a range of Pe in the regime from $\eta_{tot}$ =0.8 to $\eta_{tot}$ = 1.1, reflecting the fact that most added particles join the overlayer and only indirectly influence the base layer packing. Moreover, since the local arrangement of the base layer deviates from close-packing at the GB and features larger cavities than are present in the bulk, overlayer particles that occupy sites atop these cavities will have lower $z$ coordinates and therefore lower potential energy than those occupying sites above the ordered regions. Counting all overlayer particles, we find a positive excess number of overlayer particles per unit length of the GB, confirming that overlayer particles tend to partition towards the GB and thereby stabilize it. In this way, they are analogous to impurities in mixed systems that similarly reduce GB stiffness.[31, 38] (A kinetic effect on the GB mobility due to overlayer particles, analogous to Zener pinning,[40-42] is also possible but was not explored in the present study.) Snapshots that visualize only those overlayer particles in the range $0.5\sigma < z < 0.8\sigma$, which is excluded to particles atop closely packed hexagonal regions of the base layer, highlights the enrichment of the GB in these particles (see supporting information, Fig. S1). So, in addition to a collective pro-ordering effect of overlayer particles from their influence on the base layer's pressure, we see a pro-disordering effect from individual overlayer particles' affinity for defect sites.

Fig. 7 shows that (except for Pe=16 and Pe=18) this excess follows a regular trend with increasing coverage of the overlayer. The excess number $\Delta N/L$ increases with overlayer coverage at low $\eta_{over}$ because more particles become available to occupy the GB sites. The excess reaches a plateau as these extra-stable sites presumably become saturated. The excess number then starts to decrease as the overlayer approaches 40% monolayer coverage, as lateral packing pressure within the overlayer grows and tends to suppress local density fluctuations.

The anomalies in Fig. 7 at Pe=16 and Pe=18 can be attributed to the fact that in the regime $\eta_{over}$ =0.1-0.4 that favors high excess numbers at the GB (for reasons described in the previous paragraph) these systems are still close to their order-disorder transitions. Close to the transition point, the free energy cost of local melting in the base layer is relatively low. Overlayer particles that migrate to GB sites and stabilize non-hexagonal arrangements in the base layer can contribute to pre-melting, increasing the number of advantageous sites. In contrast, the common behaviour at higher Pe suggests that the overlayer particles are simply occupying sites determined by the intrinsic structure of the GB; the pressure in the base layer is too high to allow a significant number of additional defects to be formed. Pre-melting at the GB and an expanded zone of enrichment of overlayer particles can be seen in snapshots with Pe=16 and 18 (Fig. S1), in contrast to the localized distribution of packing defects and of overlayer particles at Pe=20.

The tendency for a partial overlayer to stabilize disordered packing arrangements in the base layer is a reasonable explanation for why $\eta_{tot}$ at the transition jumps from 0.75 at Pe=18 to over 1.1 at Pe=16 (Fig. 1). The same total pressure on the floor would be achieved with an increase only to $\eta_{tot}$=0.84. Such an increase would at the same time raise $\eta_{over}$ to approximately 0.1, a condition that strongly stabilizes defects in the base layer (Fig. 7) and so would suppress ordering. The ordered phase does not become stable until $\eta_{over}$ =0.38, and even in the ordered phase the GB stiffness is especially low at Pe=16 indicating a susceptibility to local disorder (Fig. 6).

### 3.3 Structure of ordered phase

The translational correlation function (Fig. S2) shows that the ordered phase at phase coexistence for Pe = 24 is almost the same as HD, with correlations decaying over a length scale of 10's of particle diameters as characteristic of the hexatic phase.[2] At Pe=16, even though the area packing fraction of the base layer of the ordered phase is much higher (>0.74) than for the HD system, decay of the translational order can still be observed, with a somewhat longer length scale. At Pe=6, the yet weaker decay in translational order correlation makes it difficult to identify whether the system is hexatic with a correlation length approaching the scale of the box size (350 particle diameters) or a 2-d solid with a power law correlation function. In either case, it is likely that the cooperative

 

ordering of the second layer (see following section) contributes to the increased order in the base layer.

(Pe=7) taken after 6 hours of equilibration show less order than the simulation model with Pe =6 at the same overall particle loadings.

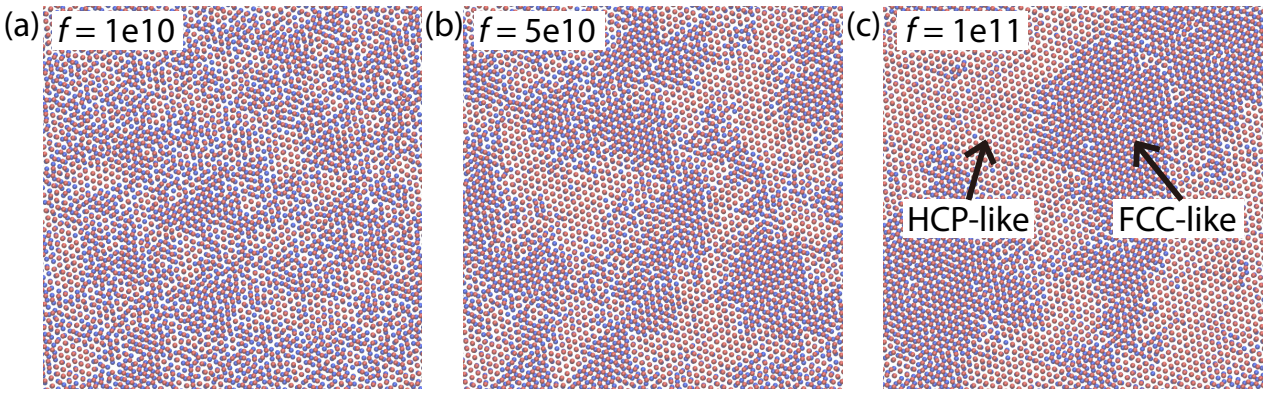


Fig. 10 Snapshot of spheres in base layer (blue) and third layer (red) in a system with Pe =6 at fugacity (a) $1 \times 10^{10}$; (b) $5 \times 10^{10}$; and (c) $1 \times 10^{11}$. The spheres in second and fourth layer are omitted for clarification. The corresponding total area fraction $\eta_{tot}$ is 2.866, 3.113 and 3.232, respectively.

As the gravitational force is lowered, the density along the *z* axis becomes more uniform, so that one might anticipate the equilibrium ordering transition at the surface to evolve from a quasi-2d process to a collective 3-d freezing that extends farther from the wall. As $\mathrm{Pe} \rightarrow 0$, one might envision that the loss of the density gradient along *z* would lead to continued expansion of this cooperativity, culminating in a bulk-like transition[35] between fluid at a volume fraction of 0.494 into a many-layered crystal at volume fractions 0.545. On the other hand, the presence of a wall has been shown to induce ordering below the bulk freezing pressure (prefreezing) in HS systems even in the absence of gravity,[43, 44] suggesting that under reduced gravity the onset of ordering will always remain local to the surface. Marechal and Dijkstra have found that at Pe=10, the base layer freezes without collective ordering of the second layer,[13] and our results are consistent with that conclusion, showing no discontinuity in the second layer order parameter at the transition point for the base layer (Fig. 8c). At Pe=8 and Pe=6 we see signs of simultaneous discontinuity in the order parameter of the first two layers, suggesting collective freezing, similar to that seen in simulations at Pe=2, 3, and 4 by Marechal and Dijkstra[13] (who also detect simultaneous ordering in the third layer at Pe=1). Particles in the second layer can populate either of two equivalently oriented lattices of trigonal holes formed by the base layer. To distinguish between those lattices, we calculate the $\Psi_3$ order parameter using the *x*-*y* projection of vectors connecting second-layer particles with the nearest three base layer particles.

$$\Psi_3(\vec{r}_j) = \frac{1}{N_j}\sum_{k=1}^{N_j} e^{i3\theta_{jk}} \qquad (14)$$

A colour map of the second layer for ordered Pe=6 systems at and above coexistence is shown in Fig. 9. These snapshots show that the second layer has only short-ranged translational order, with domains that grow gradually with increasing $\eta_{tot}$ above the transition. Note that these domains behave as stable equilibrium structures, with individual regions growing, shrinking, and changing shape over the course of each trajectory without apparent growth in average domain size.

Finally we compare results with the experiments by Ramsteiner et al.[23] Experimental images of sedimented silica microspheres

Figure 2 from ref. [23] shows grains of the order of 10s of particle diameters in dimension in the base layer at a loading of $N/A$=4.2 $\sigma^{-2}$ ($\eta_{tot}$=3.3). Domains in the second layer are well correlated with those in the base layer, without evidence of the competition between dual lattices highlighted here in Fig. 9. The third layer shows little hexagonal order until higher loadings of $N/A$ = 4.9 $\sigma^{-2}$ and 5.3 $\sigma^{-2}$. In the present simulations at Pe=6, at $\eta_{tot}$=3.23 the base layer (Fig. 10c) and second layer (data not shown) are monocrystalline while the third layer shows both HCP-like and FCC-like packing patterns,[45, 46] which are easily visualized in Fig. 10 by displaying only the first and third layers and noting where they coincide (ABA packing pattern characteristic of HCP) or are offset (ABC packing pattern characteristic of FCC). The boundaries between the domains in the third layer sometimes take the form of a double row of particles arranged as a row of squares; this feature be seen both in Fig. 10 in the present study and in Fig. 2 from ref. [23] at a higher particle loading of $N/A$ = 5.3 $\sigma^{-2}$. Discrepancies between simulation and experiment could arise from kinetic trapping of defects, from polydispersity or anisotropy effects in the real particles, or from periodic boundary artifacts in the simulations. Further simulation studies incorporating more realistic dynamics along with equilibrium properties in direct comparison with experiment will be needed to clarify the origins of these discrepancies.

## 4. Conclusions

Grand canonical Monte Carlo simulations of hard spheres confined by gravity on a flat hard surface have been carried out over a range of conditions to characterize how the 2-d ordering transition evolves when height fluctuations and overlayer effects are introduced. We have demonstrated that between Pe=18 and Pe=16, the transition shifts rapidly from a slightly perturbed 2-d ordering with a sparsely populated overlayer to a transition with a nearly 50% occupied second layer. Effects from the overlayer are complex, in that it is both a source of pressure to the base layer, favouring ordered dense packing structure, and a source of stabilization for defect sites in the base layer. The latter effect is clearly evident from the tendency of

overlayer particles to segregate towards grain boundaries in a bicrystalline model system. As the second layer is even more fully formed at the transition for lower Pe, its influence reverts to more of a mean-field blanket from above, but then becomes again involved in simultaneous ordering with the base layer below Pe=10.

In principle, the large shift in behaviour between Pe=18 and Pe=16 could be controllable in experimental systems through modest variations in solvent density or centrifugal strength. On the other hand, polydispersity will mean that particles spanning a range of Péclet numbers are likely to be present; the difference in particle diameters between Pe=18 and Pe=16 is less than 3%. This polydispersity could blunt the impact of these sharp changes, but may also introduce other phenomena of interest, and will be a topic of interest for future studies using well-established Monte Carlo methods.[47, 48]

## Conflicts of interest

There are no conflicts to declare.

## Acknowledgements

The authors thank Eric Weeks and Yijun Dong for helpful conversations. Support from the University Research Committee at Emory University is gratefully acknowledged. Peiyao Wu received support from the Emory SURE: Natural and Biomedical Sciences program. This work used the Extreme Science and Engineering Discovery Environment (XSEDE) Comet cluster at the San Diego Supercomputer Center, which is supported by National Science Foundation grant number ACI-1548562, allocation TG-MCB110144. This work also used the resources of the Cherry L. Emerson Center for Scientific Computation.

## References

1. B. Alder and T. Wainwright, *Phys. Rev.*, 1962, **127**, 359.
2. E. P. Bernard and W. Krauth, *Phys. Rev. Lett.*, 2011, **107**, 155704.
3. A. L. Thorneywork, J. L. Abbott, D. G. Aarts and R. P. Dullens, *Phys. Rev. Lett.*, 2017, **118**, 158001.
4. N. Vogel, M. Retsch, C.-A. Fustin, A. del Campo and U. Jonas, *Chem. Rev.*, 2015, **115**, 6265-6311.
5. J. Tang, P. J. Quinlan and K. C. Tam, *Soft Matter*, 2015, **11**, 3512-3529.
6. J. Wu and G. H. Ma, *Small*, 2016, **12**, 4633-4648.
7. B. P. Binks, *Langmuir*, 2017, **33**, 6947-6963.
8. T. Biben, R. Ohnesorge and H. Löwen, *Europhys. Lett.*, 1994, **28**, 665.
9. M. Marechal, M. Hermes and M. Dijkstra, *J. Chem. Phys.*, 2011, **135**, 034510.
10. S. Dorosz and T. Schilling, *J. Chem. Phys.*, 2012, **136**, 044702.
11. J. Hilhorst, D. M. de Winter, J. R. Wolters, J. A. Post and A. V. Petukhov, *Langmuir*, 2013, **29**, 10011-10018.
12. T. Palberg, *J. Phys.: Cond. Matt.*, 2014, **26**, 333101.
13. M. Marechal and M. Dijkstra, *Phys. Rev. E*, 2007, **75**, 061404.
14. J. Russo, A. C. Maggs, D. Bonn and H. Tanaka, *Soft Matter*, 2013, **9**, 7369-7383.
15. J. P. Hoogenboom, D. Derks, P. Vergeer and A. van Blaaderen, *J. Chem. Phys.*, 2002, **117**, 11320-11328.
16. J. P. Hoogenboom, P. Vergeer and A. van Blaaderen, *J. Chem. Phys.*, 2003, **119**, 3371-3383.
17. P. Pieranski, L. Strzelecki and B. Pansu, *Phys. Rev. Lett.*, 1983, **50**, 900.
18. A. Fortini and M. Dijkstra, *J. Phys.: Cond. Matt.*, 2006, **18**, L371.
19. W. Qi, A. P. Gantapara and M. Dijkstra, *Soft Matter*, 2014, **10**, 5449-5457.
20. W. Qi, Y. Peng, Y. Han, R. K. Bowles and M. Dijkstra, *Phys. Rev. Lett.*, 2015, **115**, 185701.
21. A. Sonn-Segev, J. Bławzdziewicz, E. Wajnryb, M. L. Ekiel-Jeżewska, H. Diamant and Y. Roichman, *J. Chem. Phys.*, 2015, **143**, 074704.
22. H. Choi, J. Talbot, G. Tarjus and P. Viot, *J. Chem. Phys.*, 1993, **99**, 9296-9303.
23. I. B. Ramsteiner, K. E. Jensen, D. A. Weitz and F. Spaepen, *Phys. Rev. E*, 2009, **79**, 011403.
24. J. T. Kindt, *J. Chem. Phys.*, 2015, **143**, 124109.
25. M. Schmidt and H. Löwen, *Phys. Rev. E*, 1997, **55**, 7228-7241.
26. F. Ana Barreira, S. Hans Joachim, K. Hans, P. Thomas, M. René and L. Hartmut, *J. Phys.: Cond. Matt.*, 2005, **17**, S2779.
27. S. Neser, C. Bechinger, P. Leiderer and T. Palberg, *Phys. Rev. Lett.*, 1997, **79**, 2348-2351.
28. T. Curk, A. de Hoogh, F. J. Martinez-Veracoechea, E. Eiser, D. Frenkel, J. Dobnikar and M. E. Leunissen, *Phys. Rev. E*, 2012, **85**.
29. Z. Guo and J. T. Kindt, *J. Chem. Phys.*, 2018, **149**, 044503.
30. J. I. Siepmann and D. Frenkel, *Mol. Phys.*, 1992, **75**, 59-70.
31. Z. Guo and J. T. Kindt, *Langmuir*, 2018, **34**, 12947-12956.
32. W. Humphrey, A. Dalke and K. Schulten, *J. Mol. Graph.*, 1996, **14**, 33-38.
33. V. Prasad, D. Semwogerere and E. R. Weeks, *J. Phys.: Cond. Matt.*, 2007, **19**, 113102.
34. T. Franosch, S. Lang and R. Schilling, *Phys. Rev. Lett.*, 2012, **109**.
35. W. G. Hoover and F. H. Ree, *J. Chem. Phys.*, 1968, **49**, 3609-3617.
36. A. Z. Patashinski, R. Orlik, A. C. Mitus, M. A. Ratner and B. A. Grzybowski, *Soft Matter*, 2013, **9**, 10042-10047.
37. S. Gokhale, K. H. Nagamanasa, R. Ganapathy and A. Sood, *Soft Matter*, 2013, **9**, 6634-6644.
38. F. o. A. Lavergne, S. Diana, D. G. Aarts and R. P. Dullens, *Langmuir*, 2016, **32**, 12716-12724.
39. F. A. Lavergne, D. G. A. L. Aarts and R. P. A. Dullens, *Phys. Rev. X*, 2017, **7**, 041064.
40. C. Zener, *Trans. AIME*, 1948, **175**, 15-51.
41. E. Nes, N. Ryum and O. Hunderi, *Acta Metallurgica*, 1985, **33**, 11-22.
42. G. Gottstein and L. S. Shvindlerman, *Grain boundary migration in metals: thermodynamics, kinetics, applications*, CRC press, 2009.

 

43. M. Dijkstra, *Phys. Rev. Lett.*, 2004, **93**, 108303.
44. B. B. Laird and R. L. Davidchack, *J. Phys. Chem. C*, 2007, **111**, 15952-15956.
45. V. Martelozzo, A. Schofield, W. Poon and P. Pusey, *Phys. Rev. E*, 2002, **66**, 021408.
46. M. P. Howard, W. F. Reinhart, T. Sanyal, M. S. Shell, A. Nikoubashman and A. Z. Panagiotopoulos, *J. Chem. Phys.*, 2018, **149**, 094901.
47. S. Pronk and D. Frenkel, *Phys. Rev. E*, 2004, **69**, 066123.
48. N. B. Wilding and P. Sollich, *J. Chem. Phys.*, 2002, **116**, 7116-7126.